LBL-11837 Rev.
Preprint

Lawrence Berkeley Laboratory
UNIVERSITY OF CALIFORNIA

Materials & Molecular Research Division

Submitted to Journal of Chemical Physics

OPTICAL PROPERTIES OF MOLECULES CHEMISORBED ON THE Ni(111) SURFACE

H.J. Robota, P.M. Whitmore, and C.B. Harris

August 1981

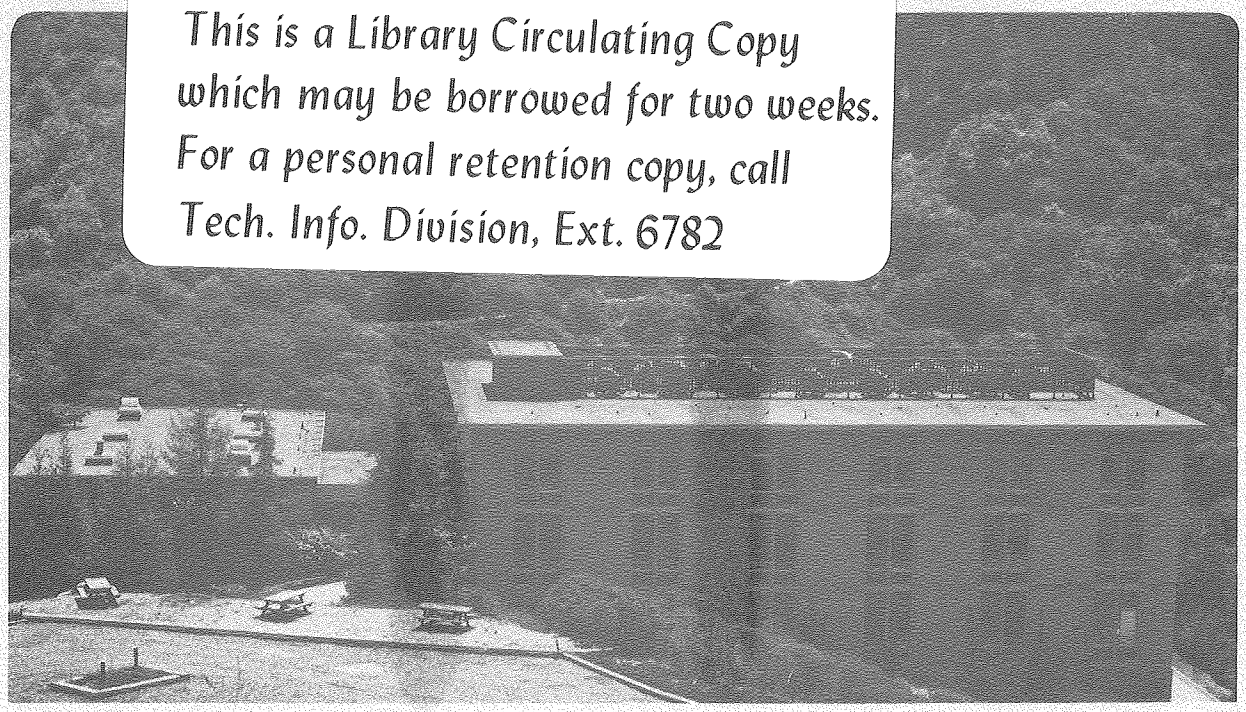

Prepared for the U.S. Department of Energy under Contract W-7405-ENG-48

DISCLAIMER

LBL #11837 Rev.
Submitted to Journal of Chemical Physics

Optical Properties of Molecules Chemisorbed on the Ni(111) Surface.

H. J. Robota, P. M. Whitmore and C. B. Harris

Department of Chemistry and Materials and Molecular Research Division of
Lawrence Berkeley Laboratory, University of California
Berkeley, California 94720

ABSTRACT

The adsorption of a series of molecules on Ni(111) is studied by UV/visible spectroscopic ellipsometry. The spectra were analyzed within a simple dielectric model. Chemisorption of molecules on the Ni(111) surface produces a peak in the overlayer optical response at 4.2 eV. This absorption peak is attributed to the selective enhancement of bulk interband excitations resulting from perturbations of the metal orbitals upon chemisorption.

This work was supported by the Division of Chemical Sciences, Office of Basic Energy Sciences of the U.S. Department of Energy under Contract No. W-7405-ENG-48.
This manuscript was printed from originals provided by the author.

I. INTRODUCTION

Significant improvement in calculation technique and experimental expertise has led to a greater understanding of the properties of atoms and molecules bound to metal surfaces. Details of the bonding interaction, energies of occupied orbitals, and the geometrical arrangement of adsorbed species can in some cases be deduced from a variety of experimental probes. Recently, the combination of optical spectroscopy with photoemission and band structure calculations has been shown to be a powerful tool for the investigation of the electronic redistribution which occurs upon chemisorption[1-3]. The success of experiments on small molecules on metal surfaces, particularly those on H_2, O_2, and CO on W[1-3] and Ni[4,5] single crystals, makes the prospect for studying the chemisorption of larger molecules very good.

Because of the importance of these endeavors to such areas as catalysis, studies of the fundamental electronic structures of large hydrocarbons chemisorbed on metal surfaces are now beginning to emerge. Of special interest is the chemisorption behavior of unsaturated and aromatic hydrocarbons. The low-lying electronic excited states of the molecular adsorbate should be very sensitive indicators of the interactions between the molecular π system and the metal. Photoemission experiments on the chemisorption of unsaturated hydrocarbons on Ni(111)[6] indicates that the electronic structures of the adsorbates remain essentially unperturbed in the bonding process, even though the molecular orbitals directly involved in the bond formation shift to somewhat higher binding energy and broaden slightly in energy. This result would suggest that the optical spectrum of a chemisorbed monolayer should resemble the free molecule spectrum of the

adsorbate, with the changes in peak energy and line width revealing details of the bonding interaction.

We have measured the visible- UV optical response of a series of molecules adsorbed on a single crystal nickel (111) surface. The molecules chosen for the initial investigation ranged from aza-aromatic hydrocarbons, which are capable of interaction through either their π systems or their nitrogen lone pairs, to aromatic hydrocarbons, expected to bond exclusively through their π systems, and finally to small molecules, which are capable of no π interactions and exhibit no strong electronic excitations in this energy region.

The results we report here indicate that the UV-visible absorption spectra for all the chemisorbed species are nearly identical, and there is no evidence of molecular-type transitions. The UV-visible spectrum of all the molecules chemisorbed on Ni(111) consists of a single peak centered at $\sim$ 4.2 eV which can be attributed to an enhancement of a bulk metal interband transition. The relationship of this transition to the band structure of nickel and the specific metal orbitals perturbed via chemisorption will be discussed.

II. EXPERIMENTAL

Apparatus

The stainless steel vacuum chamber used in these experiments is pumped by a titanium sublimation pump and a 400 ℓ/s Varian Vacion pump in the triode configuration. Typical operating pressures are $1\text{-}2\times10^{-10}$ torr as measured by an uncorrected ionization gauge. The predominant background gases are H_2, Ar, CO, and CH_4, in order of decreasing abundance as measured by a UTI 100C quadrupole residual gas analyzer. The chamber is configured in two levels. The upper level contains the liquid helium-cooled experimental stage, LEED/Auger optics, quartz entrance and exit windows, an argon ion sputtering gun, variable leak valve to a gas inlet line, and observation ports. The lower level houses the sample heating stage, a tungsten filament, residual gas analyzer, ion gauge, and additional observation ports. The sample is moved between levels with a magnetically coupled linear/rotary motion manipulator.

The nickel single crystal sample was spark cut from a 3/8" diameter rod of 99.999+% purity (Materials Research Corp.) After a preliminary orientation of the surface within 2° of the (111) face by Laue X-ray backscattering, the back was ground parallel to the face. The 1/8" thick sample was then electron beam welded to a specially machined 99.99 +% purity polycrystalline nickel backing. The sample assembly was then carefully reoriented and polished to within 1° of the (111) face. During the final polish in a slurry of .05μ Al_2O_3, the surface was swabbed at 30 minute intervals with a solution containing glacial acetic, nitric, sulfuric and phosphoric acids in relative proportion 5:3:1:1 heated to 80°C. This etching procedure removed surface layers damaged during the stages of coarse polishing.

Once in the vacuum chamber, the crystal was cleaned with several cycles of argon ion sputtering followed by extensive annealing. Typical cleaning involved 15 minutes of 2 Kv argon ion sputtering at an angle near 60° from the surface normal, 15 minutes annealing near $600^{\circ}C$, then an additional 5 minutes sputtering followed by a final anneal for 20-25 minutes. The sample was heated by lowering the crystal-backing assembly into the prongs of an insulated stage which can be raised to 5Kv above ground potential. A tungsten filament located opposite the stage was heated to produce a high flux of thermally ejected electrons which then cross the gap and strike the crystal backing. Temperature measurements were made using an optical pyrometer. Typical operating conditions were a 4Kv potential and a current of 7mA to bring the sample to $600-700^{\circ}C$. After such a cleaning procedure, LEED and Auger analysis showed highly ordered, clean nickel (111) surfaces.

During the experiments the crystal assembly was held in the copper end of a liquid helium cryostat. A secure mount was provided by mating a dovetail machined into the crystal backing with a female dovetail in the copper tip. A small leaf spring pressing on the crystal backing prevented wobbling and produced good thermal contact in the dovetail. Once in the holder, the manipulator was unscrewed from the sample. This arrangement allowed sample cooling to below 10K, as evidenced by continuous condensation of H_2 at 10^{-8}torr. Two iron-doped gold/chromel thermocouples mounted on the cold tip provided temperature estimates, but absolute measurements were prevented by the heating of secondary junctions at the vacuum feedthrough by the cryostat gas return heater.

A 75W high pressure X_e arc lamp in conjunction with a spex Doublemate monochromator equipped with ruled gratings blazed at 2500Å produced light of

sufficient intensity to 2350Å free from broadband scattered light. The light exiting the monochromator was collected with a fused silica lens, reflected from a MgF_2 coated aluminum mirror, and passed through a MgF_2 Rochon prism input polarizer onto the sample surface. The reflected light passed through the fused silica analyzer polarizer and was detected by an EMI 9558Q photomultiplier. The photomultiplier output was presented to a buffer amplifier of typical gain 100 before passing to the analog-to-digital converter for processing.

Two features of this system are considered extremely important. Both entrance and exit windows were specially constructed of UV-grade fused silica components annealed at high temperature to minimize stress-induced birefringence. The fused silica components were then attached to a pyrex graded seal on a standard vacuum flange, and, when mounted and under vacuum, display virtually no birefringence throughout the range of experimental wavelengths. The second feature, believed to be unique, is an optical path passing through holes in the LEED/Auger optics. This was accomplished by electron discharge machining to prevent warpage of the retarding grids. This arrangement allows optical studies of overlayers of known periodicity and composition, thus eliminating errors in surface adsorbate structures examined due to variations in local pressures during adsorption in separate LEED/Auger and optical spectroscopic experiments.

The spectroscopic rotating analyzer ellipsometer used in these experiments was built after a design by Aspnes. Detailed information regarding the operation, calibration, and data analysis involved in using this type of instrument may be found in references 7 and 8. Briefly, the elliptically polarized light that exits the chamber passes through a polarizer rotating at 31.25 Hz, producing a sinusoidally time-varying flux detected by the photomultiplier. The signal is sent through a buffer amplifier to an ADAC model 1030 analog-to-digital

converter interfaced to a Digital Equipment Corp. PDP11/03 laboratory microcomputer. The analysis of this signal by the computer is triggered by optical encoder circuitry on the analyzer motor. Mounted on the shaft of the rotating analyzer is a nickel-plated, polished disc with 72 parallel cuts machined at equal intervals around the circumference. At one point on the disc, an additional hole is drilled between two cut-outs. Two optical encoders are aligned with this disc to provide 72 trigger points for data collection and a single trigger acting as the origin for the data triggers.

To normalize the spectrum to the intensity of the excitation source, the photomultiplier output is monitored by Kepco APH-2000M programmable high voltage supply, and the photomultiplier voltage is adjusted so that the average DC signal level stays constant over the entire wavelength region of interest. Signal averaging is achieved by programming the computer to collect data for a specified number of revolutions of the analyzer. The monochromator is then turned to the next wavelength by a computer-controlled stepping motor, and a delay is built into the program to allow for mechanical vibrations to decay and the photomultiplier supply to adjust to the new signal level.

Data Acquisition and Reduction

Following the final annealing of the crystal, the sample assembly is moved from the heating stage to the crystal stage. The cryostat assembly is moved into the optical path and the optical components are aligned. Due to the daily movement of the sample, the angle of incidence and beam positions on the input and output windows can vary significantly. The latter is not a problem, but the former is a major difficulty which will be discussed further below. If the experiments are to be performed at low temperatures, the sample is

cooled and a final alignment of the optics is often necessary due to contractions in the cryostat. After the system has been calibrated, a spectral scan on the bare surface is performed. The gas of interest is then admitted to the chamber and progress of the adsorption is monitored ellipsometrically at a wavelength where the overlayer is presumably transparent. A second spectral scan is then collected and the two data sets can be analyzed. If further treatment of the sample are to be done, they are all performed without moving any of the system components.

While a detailed systematic discussion of ellipsometry[9, 10] is beyond the scope of this report, a brief introduction should serve as an aid to understanding the experiments and their subsequent interpretation. Linearly polarized light may be decomposed into electric field components parallel (p) and perpendicular (s) to the plane of incidence. Upon reflection from a surface, the final polarization state is, in general, elliptic due to changes in the relative amplitude and phase of the two component fields. Ellipsometry relates these changes to the complex dielectric response functions of the reflecting system. Inherent in the interpretation of ellipsometric data are a number of assumptions which for many systems appear to be reasonable. One assumes that the reflecting system can be described as a homogeneous, isotropic, semi-infinite substrate exhibiting a sharp planar boundary, covered by one or more layers of uniform thickness, also homogeneous and isotropic. This system is then embedded in some form of ambient surrounding. The applicability of this model has been challenged, especially in interpreting the behavior of thin molecular layers and sub-monolayer films on atomically clean surfaces. Several attempts have been made at describing the scattering of radiation by

atomic and molecular systems in a more rigorous fashion, yet for the general analysis of laboratory data they offer little prospect for routine applicability. Some extensions to anisotropic substrates and overlayers have been made, but they remain difficult to apply, and the bulk of ellipsometric data continues to be interpreted within this simplified framework (see reference 10).

The quantities measured in ellipsometry may be expressed as:

$$\rho = \frac{\tilde{r}_p}{\tilde{r}_s} \equiv \tan \Psi e^{i\Delta}$$

where $\tilde{r}_p$ and $\tilde{r}_s$ are the complex amplitude reflection coefficients for the electric field at the interface. In the simplified model described above, $\tilde{r}_p$ and $\tilde{r}_s$ are the Fresnel coefficients and are related to the optical properties of the overlayer, substrate and ambient, as well as the angle of incidence. For this model,

$$\frac{\tilde{r}_p}{\tilde{r}_s} = \left[\frac{\tilde{n}_1^2 \cos\phi_o - n_o(\tilde{n}_1^2 - n_o^2 \sin^2\phi_o)^{1/2}}{\tilde{n}_1^2 \cos\phi_o + n_o(\tilde{n}_1^2 - n_o^2 \sin^2\phi_o)^{1/2}}\right]\left[\frac{\tilde{n}_o \cos\phi_o + (\tilde{n}_1^2 - n_o^2 \sin^2\phi_o)^{1/2}}{\tilde{n}_o \cos\phi_o - (\tilde{n}_1^2 - n_o^2 \sin^2\phi_o)^{1/2}}\right]$$

where $\tilde{n}_o$ is the refractive index of the ambient, $\tilde{n}_1$ is the complex refractive index of the substrate, and ϕ_o is the angle of incidence with respect to the substrate normal. For any layered system, the Fresnel coefficients for a given layer j can be determined as

$$\tilde{r}_{jp} = \frac{\tilde{n}_j \cos\phi_{j-1} - \tilde{n}_{j-1} \cos\phi_j}{\tilde{n}_j \cos\phi_{j-1} + \tilde{n}_{j-1} \cos\phi_j}$$

$$\tilde{r}_{js} = \frac{\tilde{n}_{j-1} \cos\phi_{j-1} - \tilde{n}_j \cos\phi_j}{\tilde{n}_{j-1} \cos\phi_{j-1} + \tilde{n}_j \cos\phi_j}$$

where now all refractive indices and angles are, in general, complex. For the

systems to be dealt with here, the three phase (ambient-overlayer-substrate) ellipsometric equation can be expressed as

$$\rho = \tan\Psi_e^{\,i\Delta} = \left[\frac{r_{1p}+r_{2p}e^{-iZ}}{1+r_{1p}r_{2p}e^{-iZ}}\right]\left[\frac{1+r_{1s}r_{2s}e^{-iZ}}{r_{1s}+r_{2s}e^{-iZ}}\right]$$

$$Z = (4\pi d/\lambda o)\ (\tilde{n}_1^2 - n_o^2 \sin^2\phi_o)^{1/2}$$

where d is the thickness of the overlayer and λo is the vacuum wavelength of light. For all of the results presented here, the incident beam was about 60^o from the surface normal and linearly polarized at 30^o from the plane of incidence.

Unlike classical null ellipsometers, rotating analyzer systems of this type measure $\tan\Psi$ and $\cos\Delta$ rather than Ψ and Δ directly. For the metal systems investigated, the expected values of Ψ and Δ are such that there is no ambiguity in converting from ($\cos\Delta$, $\tan\Psi$) to (Δ,Ψ) for further analysis. The simplest type of analysis consists of the difference between bare metal parameters ($\bar{\Delta}$,$\bar{\Psi}$) and the corresponding values for the covered metal at each point in the spectrum. The difference functions $\delta\Psi=\Psi-\bar{\Psi}$ and $\delta\Delta=\Delta-\bar{\Delta}$ (the bar indicating bare metal values) are, in general, complicated functions of the overlayer dielectric properties and thickness. However, experience has shown that most of the spectral features can be gleaned from these simple functions without resorting to sophisticated analyses. Figure 1a shows the result of $\delta\Delta$ and $\delta\Psi$ for a 10Å layer of condensed annealed pyrazine. For comparison, 1 b demonstrates the result of analyzing for n and k. These spectra also demonstrate the sensitivity of the instrument for moderate and strong absorption features in very thin layers. (Notice the resolved vibronic structure in the low energy transition.) As a standard tool, difference spectra are not usually used to interpret spectral data. They

are extremely useful, though, in regions where the overlayers are transparent, where $\delta\Psi \simeq 0$ and $\delta\Delta \propto d/\lambda o$, so that the change in Δ can be used as a crude measure of the thickness of the overlayer during an adsorption.

Two factors in these experiments make rigorous analyses of the spectra difficult. The first involves uncertainty in the angle of incidence. For a given dielectric constant and wavelength of light, variations in the angle of incidence by as little as 0.01° have pronounced influence on the values of Ψ and Δ. Due to the nature of our sample mount, variations in the angle of incidence as large as 1° arise on a daily basis. Measurements of this angle are subject to errors of approximately $\pm 0.1^{\circ}$. Thus, the values of optical constants resulting from the analysis must not be regarded as absolute but used for defining spectral features and as a means of comparison between systems.

The second uncertainty in the analysis is in the thickness of the overlayer. Complete characterization of the overlayer requires three parameters: the real and imaginary parts of the refractive index, and the thickness of the layer. Ellipsometric measurements provide only two pieces of information, so a third measurement must be made or inferred. The most common solution is to make an ellipsometric measurement where the overlayer is assumed transparent. The remaining variables, n and d, can be uniquely determined, and the calculated thickness can then be used to calculate both n and k at other wavelengths. A second method[11] involves making measurements of Ψ and Δ at several thicknesses during the course of a deposition. A series of solutions over a range of n and k values is calculated which make the thickness a purely real quantity. When the solutions for two different thicknesses are plotted in n-k space, the intersections of the curves correspond to the

n and k values shared by both measurements. If the assumption is made that these n and k values are constant for all thicknesses, then the thickness of the overlayer at the end of the adsorption run can be calculated and used in the determination of n and k at different wavelengths. This approach has proven to be useful for a number of condensed layer systems, but for very thin layers and chemisorbed systems, this method has been found to be unreliable. The solution to this problem which was finally adopted in our analysis is a cautious comparison of the thickness of the overlayer expected from exposure times and molecular dimensions with that obtained by minimizing the absorption index in a region of expected transparency.

The frequency dependent complex refractive index represents the desired information about the response of the adsorbed overlayer, and the method used to obtain these values is straightforward. Each experimental spectrum terminates in a region where the overlayer is expected to be transparent. The values of Ψ and Δ measured for the bare and covered surface are used in a linear approximation expansion of the exact ellipsometric equations, which are applicable to layers where $d \ll \lambda$[10]. An initial guess is made for d and the complex refractive index is calculated. Successive values for d are examined until k is minimized. This value of the complex refractive index and thickness are then used in an iteration scheme based on a Taylor expansion of ρ in the complex refractive index. Iterations are performed until the deviation of the calculated ρ values from measured ρ values is within expected experimental error. This represents the first value of the overlayer refractive index. The next point in the spectrum is analyzed in the same way, using the best fit refractive index from the previous point as the starting value for the iteration. The complex index is calculated

at each point in the spectrum, and the final results are plotted as n and k vs. λ . Experience has shown that while the absolute values of n and k have a strong dependence on the chosen film thickness, the features in the spectrum remain undistorted until obviously erroneous thicknesses are used.

III. RESULTS

The studies of chemisorbed molecules were all performed at room temperature except where otherwise noted. Gases were deposited at pressures in the 10^{-8} torr range for several minutes until saturation occurred as measured by the change in the ellipsometric parameter Δ. Auger and LEED results were obtained after the ellipsometric spectra were recorded to minimize the effects of electron beam damage to the overlayers.

Condensed layers of gases were prepared by adsorption while the crystal was cooled to 15K. Thicknesses were monitored ellipsometrically, and in some cases the overlayers were annealed at 150K and cooled back to 15K before spectra were taken.

All the ellipsometric spectra were recorded with 0.5mm slits on the monochromator (10Å passband) and the data points were taken at 5Å intervals. Each point was averaged over 200 revolutions of the analyzer.

Pyrazine, Pyridine, Benzene, and Naphthalene on Ni(111)

The analyzed ellipsometric spectra of annealed condensed layers of pyrazine, pyridine, and naphthalene on Ni(111) at 15K are shown in Figures 2-4. Intense absorption peaks with vibronic structure are evident. The spectrum of a thick layer of condensed benzene showed no absorption maxima in this wavelength region, only the apparent onset of a large peak at higher energies. These spectra establish the positions of the molecular absorptions in the adsorbed layer and will be useful in interpreting the spectra of the corresponding chemisorbed species.

Pyrazine, pyridine, benzene, and naphthalene all appear to chemisorb on Ni(111) at room temperature. Saturation of the surface occurs after 3-5L exposures, with a final $\delta\Delta$ of about 0.5° - 0.7° at 3500Å. The adsorption of

pyridine leads to a very diffuse LEED pattern visible only at low electron energies (figure 5). LEED spots for the chemisorbed pyrazine were very indistinct and subject to very rapid deterioration in the electron beam. Naphthalene on the other hand produces very clear, reproducible patterns which would deteriorate after longer beam exposures. From an initial set of rings surrounding each clean surface spot, annealing to 350K produces the pattern seen in figure 6. Although we make no assignment of these patterns, similar results were obtained on the Pt(111) surface.[12]

The spectrum of each of these chemisorbed molecules is shown in Figures 7-10. Each absorption spectrum is dominated by one large, broad feature, which is centered at 2850Å in the case of pyrazine and benzene, and at 3050Å for chemisorbed pyridine and naphthalene. None of the molecules studied exhibited any absorption features in the visible region of the spectrum.

CO, O_2, Ethanol on Ni(111)

The chemisorption of CO on Ni(111) yielded the familar LEED pattern[13] after saturation at 3L. The final $\delta\Delta$ was 0.6° monitored at 3000Å. The UV absorption spectrum is shown in Figure 11 and consists of a large, broad peak centered at 2800Å.

Adsorption of O_2 at room temperature appears to undergo a rapid chemisorption phase ($\delta\Delta \sim 0.2^\circ$ at 5000Å, p(2x2) LEED pattern develops after 1.5L). After this initial stage, a slow oxygen uptake is indicated by the ellipsometer, with a final $\delta\Delta \sim 2.0^\circ$ and a LEED pattern characteristic of NiO after 300L. The analyzed spectrum of chemisorbed O_2 is shown in figure 12, and again a broad feature at 2900Å is prominent. Prolonged exposure to form the NiO

had two effects on the analyzed spectrum. The magnitude of the analyzed peak was markedly increased and the actual peak position was shifted to higher energy as seen in figure 13.

At room temperature, exposure of the crystal to ethanol leads to a disordered chemisorbed phase, with $\delta\Delta \simeq 0.3^{\circ}$ at 5000Å. The absorption spectrum of this species is shown in figure 14 and exhibits a peak at 2750Å. For comparison, a spectrum of a 100Å thick layer of ethanol condensed on Ni(111) at 80K is shown on the same scale. No evidence of an absorption peak is visible in the condensed layer spectrum.

IV. DISCUSSION

The electronic absorption spectra of thick, annealed layers of pyrazine, pyridine, and naphthalene condensed on Ni(111) show intense peaks with sharp vibronic structure. As previously reported for pyrazine on Ni(111)[14], the peak energies and vibrational spacings agree well with those reported for the respective bulk crystals. The intense absorption peaks which occur near 2700Å in the spectra of pyrazine and pyridine are attributed to $\pi\pi^*$ excitations ($^1B_{2u}$ and $^1B_2$ respectively)[15]. Similarly, the absorption band in the spectrum of naphthalene is derived from two $\pi\pi^*$ transitions, $^1B_{3u}$ and $^1B_{2u}$[16]. The additional feature in the condensed pyrazine spectrum at 3300Å corresponds to an $n\pi^*$ excitation out of a nitrogen lone pair molecular orbital. This good correspondence with bulk crystal transition energies and vibrational spacings indicates that, for the case of weak interaction with the metal, the adsorbed molecules retain their molecular electronic structure and are only slightly perturbed by the metal surface.

In contrast to this behavior, the formation of a chemisorption bond has a very pronounced effect on the optical spectrum. All traces of the molecular transitions which appeared for the condensed payers are lost, and a single intense, broad absorption band centered between 2800Å and 3100Å (∿4.2 eV) dominates the UV spectrum. This absorption appears at approximately the same energy and with the same shape for all the chemisorbed species studied, suggesting that a feature of the chemisorption process, rather than the molecular properties of the adsorbate, is responsible for the observed absorption peak. In light of the strong interband excitations for the bulk nickel in this energy range[17], it is likely that this spectral

feature originates in chemisorption-induced modifications in the optical response of the metal substrate.

Previous reflectance work on H_2, O_2, and CO on W(110)[1] yielded a very similar result: enhanced absorption at the energies of bulk interband transitions, accompanied by removal of lower energy transitions which appear in the clean metal spectrum. This behavior was attributed to a chemisorption-induced quenching of W(110) surface resonances (which were the initial states of the low-energy transitions), accompanied by a rehybridization of bulk bands, thus changing the interband matrix elements slightly and enhancing bulk excitation intensities. This analysis was supported by UPS data and theoretical calculations demonstrating the existence of these surface resonances[1], and by subsequent studies of the anisotropy of the optical response of the adsorbate-covered surface[2].

This same mechanism has been used to explain effects of chemisorption on photoemission from Ni(111)[4,18]. Chemisorption of H_2, O_2, CO, etc. causes electron emission from an sp_z-like Λ_1 surface state (0.25 eV below E_F on the clean surface) to shift to higher binding energy with increasing coverage and eventually disappear. At the same time electron emission from two sp-like Λ_1 bulk bands increases. This is interpreted as a mixing of adsorbate orbitals with the tails of bulk bands at the surface (the Λ_1 bulk bands having significant electron density in the surface region), causing both the removal of the surface state and the rehybridization which increases the interband matrix elements for excitations out of the Λ_1 bulk states. The d-like Λ_3 bulk state is affected very little in this process, suggesting little participation of Ni d-orbitals in the chemisorption

bonding. Strong interaction of adsorbate orbitals with the Ni s-band would also lead to a highly delocalized adsorbate band spread out many eV in energy, and this is supported by the absence of emission from an adsorbate-like bonding orbital.

We believe that the chemisorption-induced feature which we observe in the optical spectrum at 4.2 eV is a direct result of this same rehybridization of the Λ_1 s-band that is indicated in the photoelectron spectrum taken at $\sim$20 eV. Although there are many interband contributions to this region of the nickel absorption spectrum, band structure calculations[19,20] support the assignment of an optical transition at $\sim$4.5 eV to a $\Lambda_1 \rightarrow \Lambda_3$ excitation (i.e., out of the lower sp-like state), near the L point in the 3-D Brillouin zone (the [111] direction). This is illustrated in Fig. 15. Just as in the photoemission experiments, rehybridization of this Λ_1 state upon chemisorption would change the $\Lambda_1 \rightarrow \Lambda_3$ matrix element, thus enhancing this bulk transition.

Of the many contributions to the bulk nickel spectrum in this region, only the $\Lambda_1 \rightarrow \Lambda_3$ transitions near the L point seem to be enhanced upon chemisorption. This can be rationalized in terms of a rehybridization of the Λ_1 (sp_z-like) states to increase the p_z character of the state (z direction along the surface normal) near the surface as a chemical bond to an adsorbate is formed. Such an increase in p character might lead to better overlap with the d-like Λ_3 final state, thus increasing the intensity of these transitions. Excitations from the sp-like Δ_1 states near the X-point (in the [100] direction), which should occur near 3.5 eV, are not enhanced upon chemisorption, probably because the bond formation does not require significant hybridization in the [100] direction. Thus,

the chemisorption process seems to selectively enhance transitions from the nickel sp-like bands along the direction of the surface normal.

Another feature of the optical spectra which is particularly striking in comparing the spectra of the condensed and chemisorbed aromatic hydrocarbons is the disappearance of quite strong molecular transitions upon chemisorption. None of the intense $\pi\pi^*$ absorptions (nor the weaker $n\pi^*$ of pyrazine), which are prominent in the absorption spectra of even very thin condensed layers, can be seen in the spectra of the respective chemisorbed species. In the related photoemission work on Ni(111)[4], Himpsel, Knapp, and Eastman (HKE) claim that there are no resonances from adsorbate valence orbitals in the photoelectron spectra of H_2 and O_2 on Ni(111) because the adsorbate bonding orbital interacts so strongly with the s-band of the metal that it disperses in energy over the entire width of the s-band (~6 eV wide). However, earlier photoemission results of hydrocarbons chemisorbed on Ni(111) by Demuth and Eastman (DE)[6] were used to demonstrate that the molecular orbitals of the adsorbate, even those involved with bond formation, remain essentially intact after chemisorption. Those adsorbate bonding orbitals seem to shift to higher binding energy and to broaden slightly. However, our results and those of HKE, which indicate strong s-band contributions to the chemisorption process, seem to be at odds with the DE picture.

We believe that our results and the ARUPS results of HKE are consistent with the data presented by DE, but not with their interpretation of the data. A closer examination of the DE photoelectron spectra shows first the decrease in electron emission just below the Fermi energy which is now known to be due predominantly to the removal of the Λ_1 surface state on the (111)

surface of nickel (although very slight perturbations in the d-band emission might also be represented). In addition to the electron emission from the many low-lying adsorbate levels which seem relatively unperturbed from the gas phase, there is a broad resonance which occurs at ~5 eV below E_F for all the adsorbates. DE assign this electron emission peak to an adsorbate π orbital which, after interaction with the metal, shifts to higher binding energy relative to the gas phase. However, our results and those of HKE, which imply the presence of this resonance even for adsorbates which do not have a nearby valence orbital, strongly suggest that this feature is in fact the enhanced electron emission from the lower Λ_1 state of the substrate, and not due to a molecular adsorbate level. If this interpretation is correct, then the electron emission from the adsorbate bonding orbital is not represented in the photoelectron spectrum, or is at least so broad as to be unresolved. These bonding orbitals, the π levels of the unsaturated hydrocarbons, which would have been the initial states for the lowest energy optical excitations, would thus be broadened greatly so that the corresponding absorption peaks would not be visible, as is the case for the systems we have studied.

The removal of the Λ_1 surface state, the enhancement of the Λ_1 bulk states, and the severe broadening of the adsorbate bonding levels, are all consistent with the picture of nickel bonding mainly through its s-like band states. If our analysis of the photoelectron spectra of unsaturated hydrocarbons on Ni(111) is correct, the adsorbates interact with the metal mainly through their π systems (with possible contributions from the nitrogen lone pairs in the heteronuclear aromatics). The s-band participation in the chemisorption process has been proposed previously[4,21,22], especially in comparisons with chemisorption on Pd or Pt, where the d-bands play a much

larger role. Bonding of unsaturated hydrocarbons through their π systems has also been supported by a wide variety of studies[21-24].

Naturally the d-band of Ni must participate to some extent in the chemisorption process even though in the cases studied s-band contirbutions seem to dominate. The degree of d-band character in the chemisorption bond should vary with different adsorbates, and should be reflected in the optical spectrum. Two features should indicate strong d-band interactions: perturbations of interband excitations from d-like states, and the appearance of molecular transitions in the absorption spectrum, since the adsorbate bonding orbital should not be broadened greatly upon interaction with the d-band. In fact, recent photoemission studies of H_2/Ni(111)[5] indicate that there exists a low-temperature phase in which the nickel d-bands appear to play a larger role in the formation of the chemisorption bond, as determined from large changes in the emission from the d-band states and from the appearance of a resonance at 9 eV below E_F attributed to the H orbital. Similar d-band contributions have been noted for CO/Ni(111)[13].

Such dramatic changes in electronic structure must surely be apparent in the optical spectrum at the appropriate energies. We cannot, unfortunately, probe the spectral regions of interest here because we are limited to working in the visible-near UV. However, Rubloff and Freeouf[25] have investigated CO/Ni(111) at higher energies using surface reflectance and electron loss measurements. In addition to a peak in the ELS at ∿4 eV, which we can now assign to an enhanced metal interband transition, there is an absorption near 8 eV which could correspond, as they suggest, to the $X^1\Sigma^+ \rightarrow A^1\Pi$ of molecular CO (i.e., a $5\sigma \rightarrow 2\pi^*$ excitation). This indicates d-band interaction in addition to s-band contributions, which is consistent with the picture of CO

bonding through the 5σ orbital on carbon with back-bonding from the metal d-states into the $2\pi^*$. Optical investigations of the perturbations of these metal d-states should provide more information on the details of this bonding interaction.

V. CONCLUSION

We have studied the optical response of molecules chemisorbed on Ni(111) surfaces in the visible-near UV region. The observed absorption peak at 4.2 eV is assigned to a selective enhancement of the $\Lambda_1 \rightarrow \Lambda_3$ interband excitation near the L-point of the Brillouin zone. (i.e., in the direction of the surface normal). Our results suggest that the π orbitals of the aromatic hydrocarbons (and perhaps the nitrogen lone pairs in the azabenzenes) interact strongly with the nickel s-band states in forming the chemisorption bond.

VI. ACKNOWLEDGEMENT

This work was supported by the Division of Chemical Sciences, Office of Basic Energy Sciences, U. S. Department of Energy under contract No. W-7405-Eng-48.

References

1. G. B. Blanchet and P. J. Stiles, Phys. Rev. B 21, 3273 (1980), and references therein.

2. G. B. Blanchet, P. J. Estrup, and P. J. Stiles, Phys. Rev. B 23, 3655 (1981).

3. J. B. Restorff and H. D. Drew, Surf. Sci., 88, 399 (1979).

4. F. J. Himpsel, J. A. Knapp, and D. E. Eastman, Phys. Rev. B 19, 2872 (1979).

5. W. Eberhardt, F. Greuter, and E. W. Plummer, Phys. Rev. Lett., 46, 1085 (1981).

6. J. E. Demuth and D. E. Eastman, Phys. Rev. Lett., 32, 1123 (1974).
J. E. Demuth and D. E. Eastman, Phys. Rev. B 13, 1523 (1976).

7. D. E. Aspnes and A. A. Studna, App. Opt. 14, 220 (1975).

8. D. E. Aspnes, J. Opt. Soc. Am., 64, 812 (1974).

9. D. E. Aspnes, "Spectroscopic Ellipsometry of Solids," in Optical Properties of Solids: New Developments, B. O. Seraphin, ed., North-Holland, 1976.

10. R. M. A. Azzam and N. M. Bashara, Ellipsometry and Polarized Light, North-Holland, 1977.

11. M. Malin and K. Vedam, Surf. Sci., 56, 49 (1976).

12. J. L. Gland and G. A. Somorjai, Surf. Sci., 38, 157 (1973).

13. H. Conrad, G. Ertl, J. Kuppers, and E. E. Latta, Surf. Sci., 57, 475 (1976) and references therein.

14. C. B. Harris, D. A. Zwemer, A. R. Gallo, and H. J. Robota, Surf. Sci., 85, L205 (1979).

15. K. K. Innes, J. P. Byrne, and I. G. Ross, J. Mol. Spec., 22, 125 (1967) and references therein.

16. D. S. McClure and O. Schnepp, J. Chem. Phys., 23, 1575 (1955).

17. D. S. Laurent, J. Callaway, and C. S. Wang, Phys. Rev. B 20, 1134 (1979).

18. F. J. Himpsel and D. E. Eastman, Phys. Rev. Lett., 41, 507 (1978).

19. C. S. Wang and J. Callaway, Phys. Rev. B 15, 298 (1977).

20. L. C. Davis and L. A. Feldkamp, Sol. State Comm., 34, 141 (1980).

21. J. E. Demuth, Surf. Sci., 65, 369 (1977).

J. E. Demuth, Surf. Sci., 76, L603 (1978).

22. S. Lehwald and H. Ibach, Surf. Sci., 89, 425 (1979).

23. S. Lehwald, H. Ibach, and J. E. Demuth, Surf. Sci., 78, 577 (1978).

24. J. C. Bertolini and J. Rousseau, Surf. Sci., 89, 467 (1979).

J. C. Bertolini, G. Dalmai-Imelik, and J. Rousseau, Surf. Sci., 67, 478 (1977).

25. G. W. Rubloff and J. L. Freeouf, Phys. Rev. B 17, 4680 (1978).

Figure Captions

Figure 1 a: The result of a simple difference spectrum ($\delta\Delta,\delta\Psi$) for a 10Å thick, condensed and annealed layer of pyrazine on Ni(111). $\delta\Psi$ reflects the absorbing properties of the layer while $\delta\Delta$ is most sensitive to the refractive index.

Figure 1 b: Absorbance calculated from an iterative analysis assuming a 10Å thick layer. Compare the vibronic structure with that of a thick layer in figure 2.

Figure 2: The analyzed absorption spectrum for a 40Å thick condensed, annealed pyrazine layer on Ni(111).

Figure 3: The analyzed absorption spectrum for a 65Å thick condensed, annealed layer of pyridine on Ni(111).

Figure 4: The analyzed absorption spectrum for a 25Å thick condensed, annealed layer of naphthalene on Ni(111).

Figure 5: The LEED pattern of pyridine chemisorbed on Ni(111) at room temperature. The beam energy is 66eV. (a) Photograph of the diffraction pattern. (b) Sketch of the pattern. Nickel diffraction spots are indicated by solid circles. Spots due to chemisorbed pyridine are indicated by the open outlines.

Figure 6: The LEED pattern of naphthalene chemisorbed on Ni(111) at room temperature after annealing at 80°C. The beam energy is 52eV. (a) Photograph of the diffraction pattern. (b) Sketch of the pattern. Nickel diffraction spots are indicated by solid circles. Spots due to chemisorbed naphthalene are indicated by solid and open ovals.

Figure 7: The analyzed absorption spectrum for chemisorbed pyrazine on Ni(111).

Figure 8: The analyzed absorption spectrum for chemisorbed pyridine on Ni(111).

Figure 9: The analyzed absorption spectrum for chemisorbed benzene on Ni(111).

Figure 10: The analyzed absorption spectrum for chemisorbed naphthalene on Ni(111

Figure 11: The analyzed absorption spectrum for chemisorbed CO on Ni(111).

Figure 12: The analyzed absorption spectrum for chemisorbed oxygen on Ni(111).

Figure 13: The analyzed spectrum of epitaxial NiO formed after prolonged exposure of the Ni(111) surface to oxygen.

Figure 14: The analyzed absorption spectra of chemisorbed ethanol (upper curve) and a 100Å layer of condensed ethanol (lower curve), shown on the same scale for comparison.

Figure 15: Calculated band structure of nickel including electron correlation, taken from Ref. 20 (only the minority spin bands are shown.). The lowest Λ_1 band is predominantly S-like, with significant P_z character near the L point (z in the direction of the surface normal). The highest Λ_3 band is mainly d-like. The arrow indicates the interband transition at 4.2 eV which is enhanced upon chemisorption.

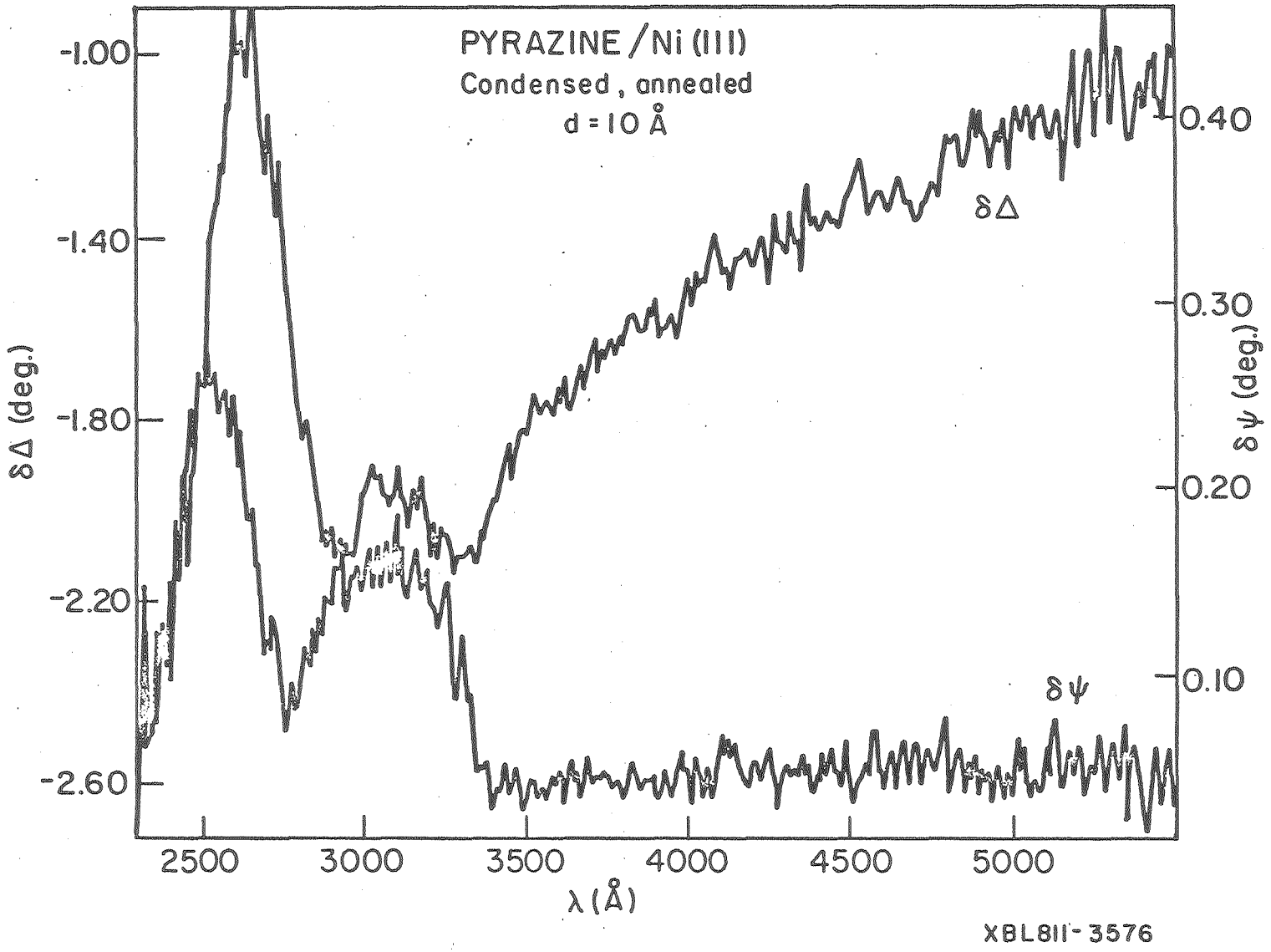
PYRAZINE / Ni (111)
Condensed, annealed
d = 10 Å
δΔ
δψ
-1.00
-1.40
-1.80
-2.20
-2.60
δΔ (deg.)
0.40
0.30
0.20
0.10
δψ (deg.)
2500
3000
3500
4000
4500
5000
λ (Å)
XBL811-3576

Figure 1a

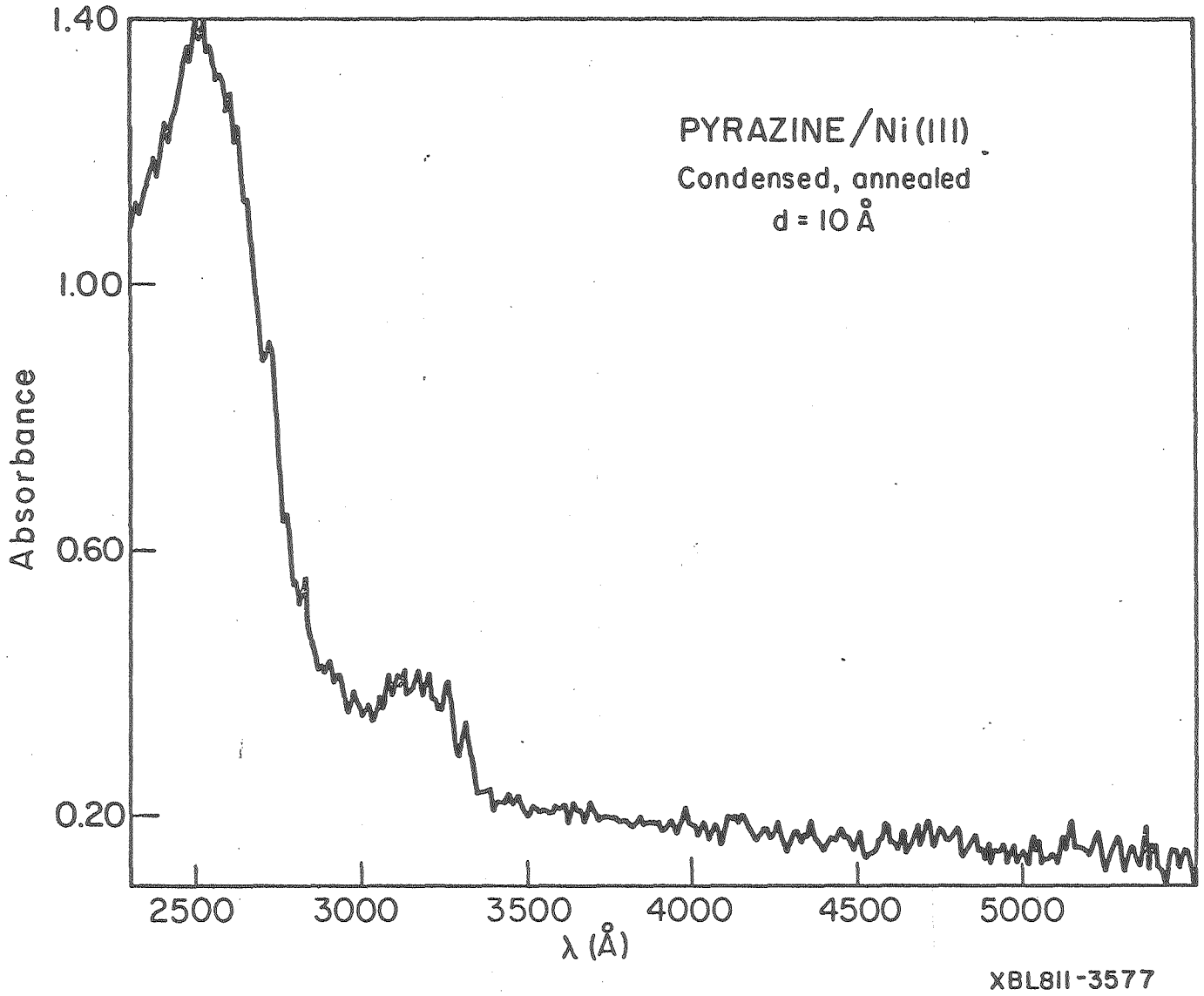
1.40
1.00
0.60
0.20
Absorbance
PYRAZINE/Ni(111)
Condensed, annealed
d = 10 Å
2500
3000
3500
4000
4500
5000
λ (Å)
XBL811-3577

Figure 1b

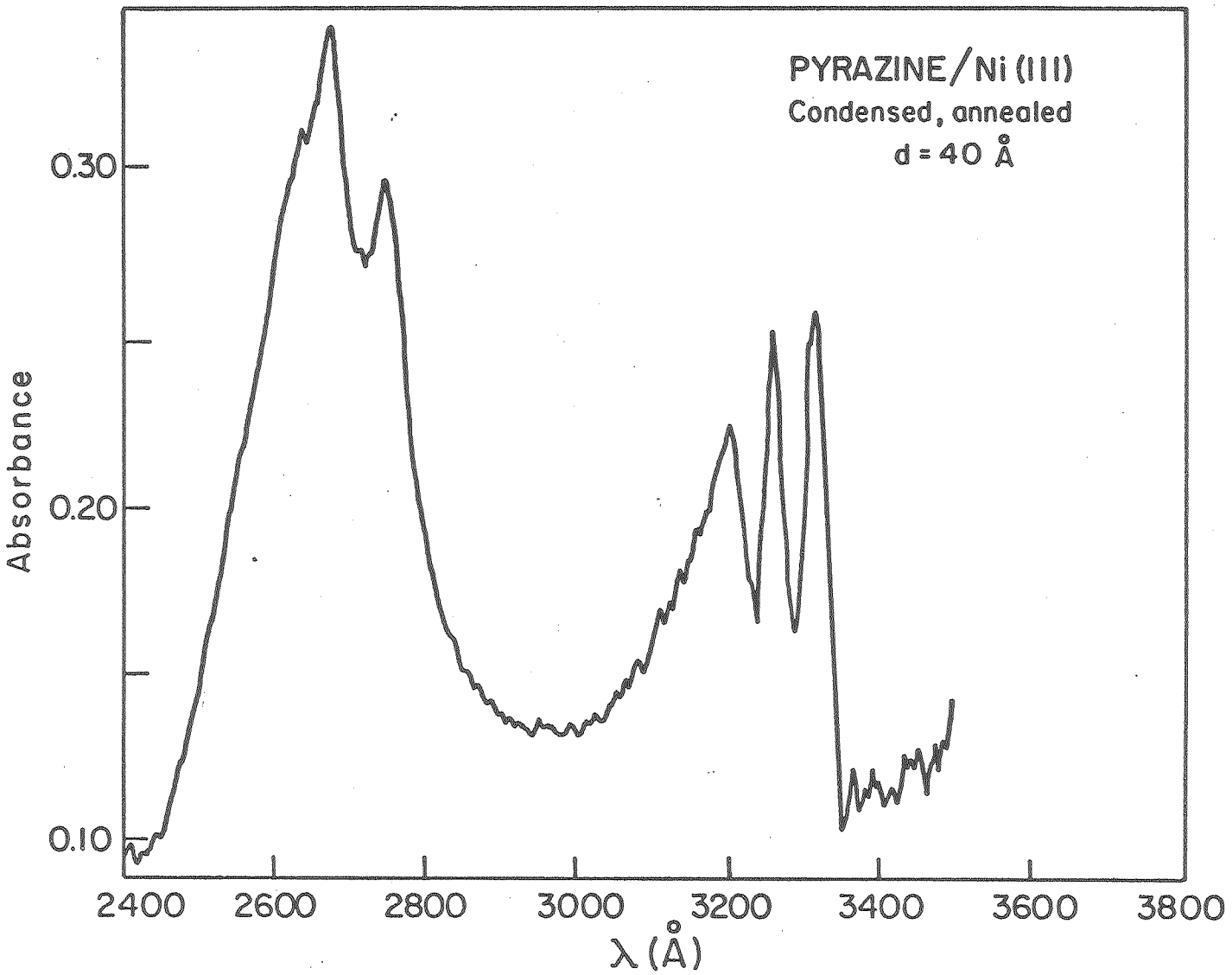
PYRAZINE/Ni (111)
Condensed, annealed
d = 40 Å
Absorbance
0.30
0.20
0.10
2400
2600
2800
3000
3200
3400
3600
3800
λ (Å)
XBL806-5330

Figure 2

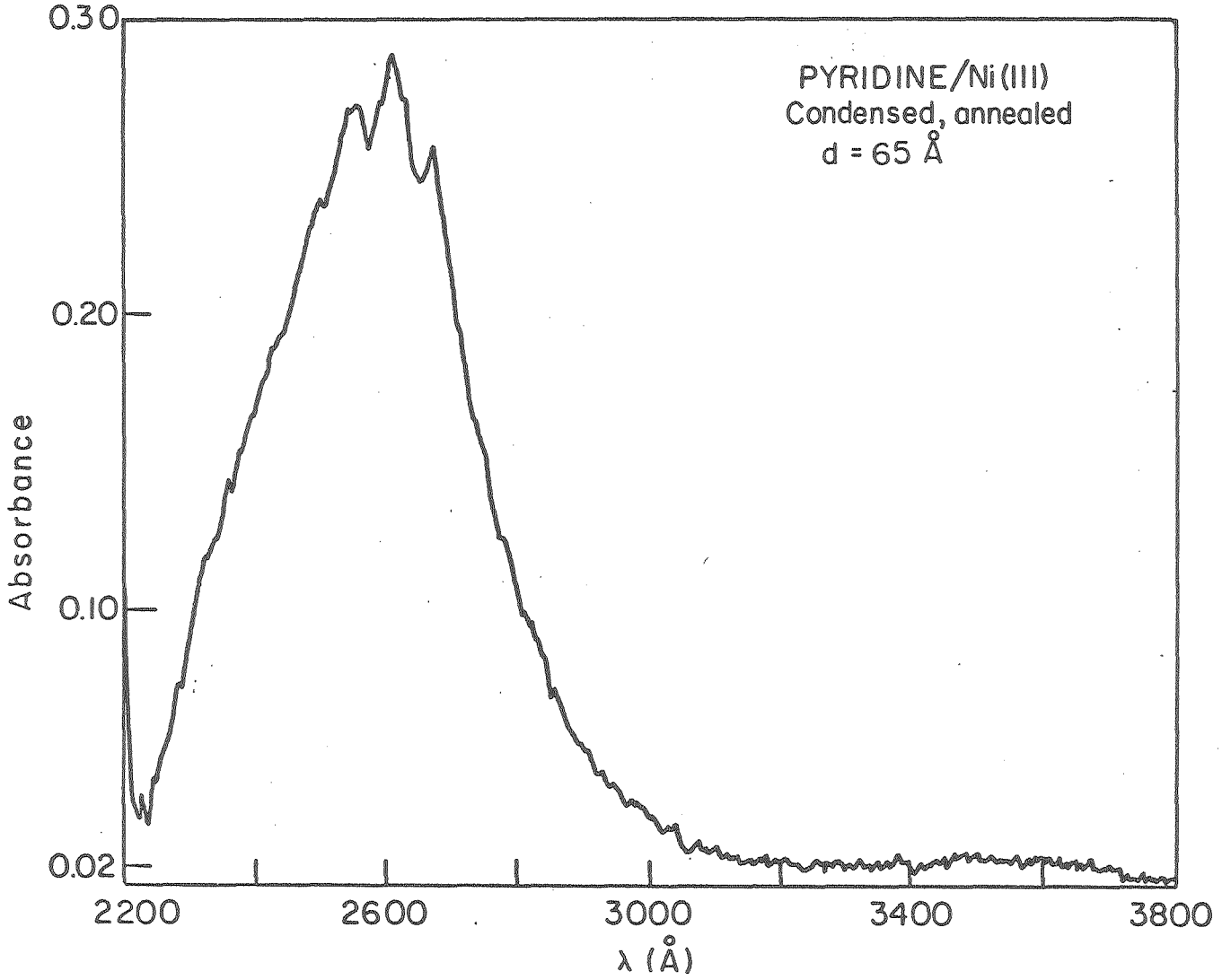
PYRIDINE/Ni(111)
Condensed, annealed
d = 65 Å
0.30
0.20
0.10
0.02
Absorbance
2200
2600
3000
3400
3800
λ (Å)
XBL811-3575

Figure 3

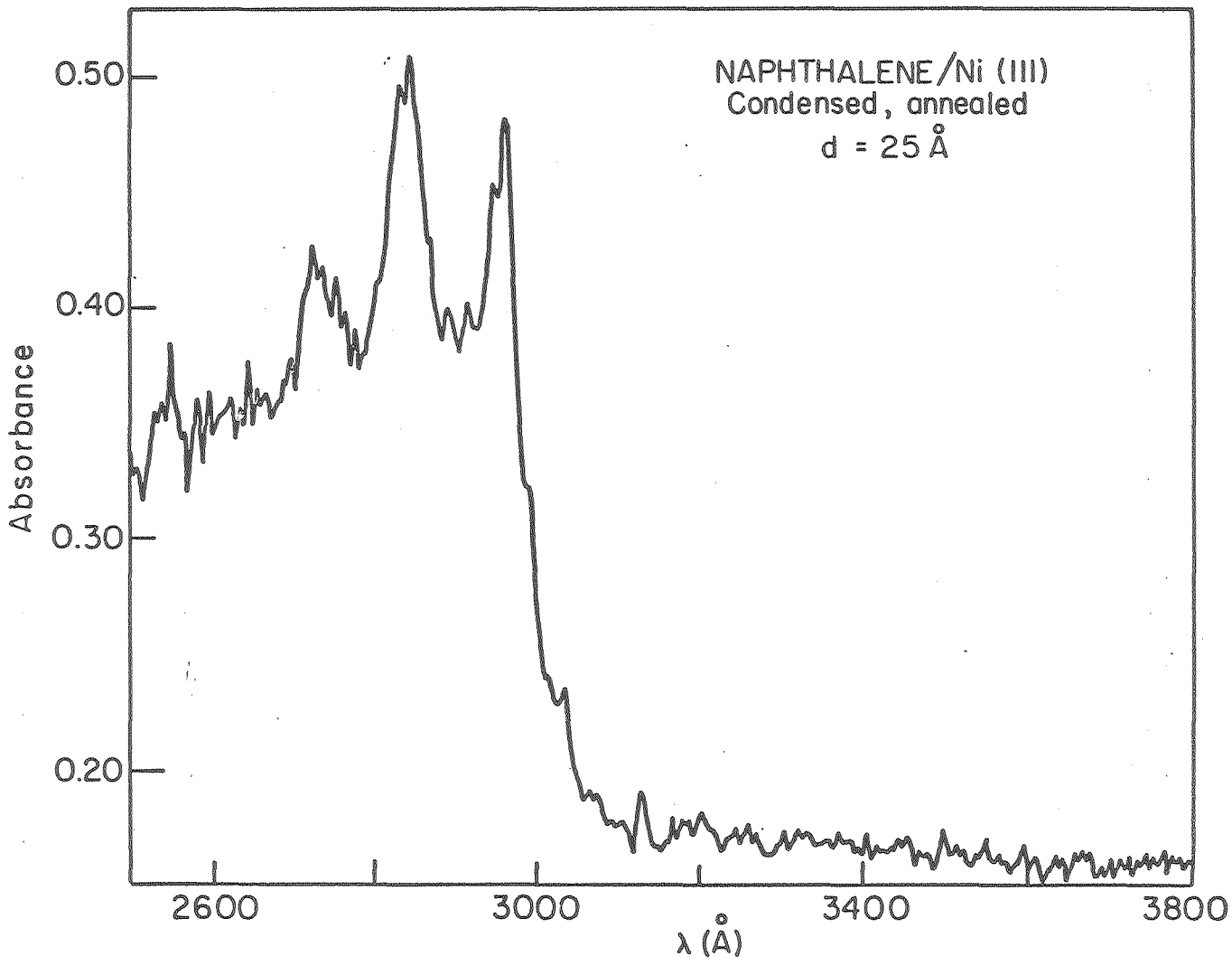
NAPHTHALENE/Ni (III)
Condensed, annealed
d = 25 Å
0.50
0.40
0.30
0.20
Absorbance
2600
3000
3400
3800
λ (Å)
XBL811-3574

Figure 4

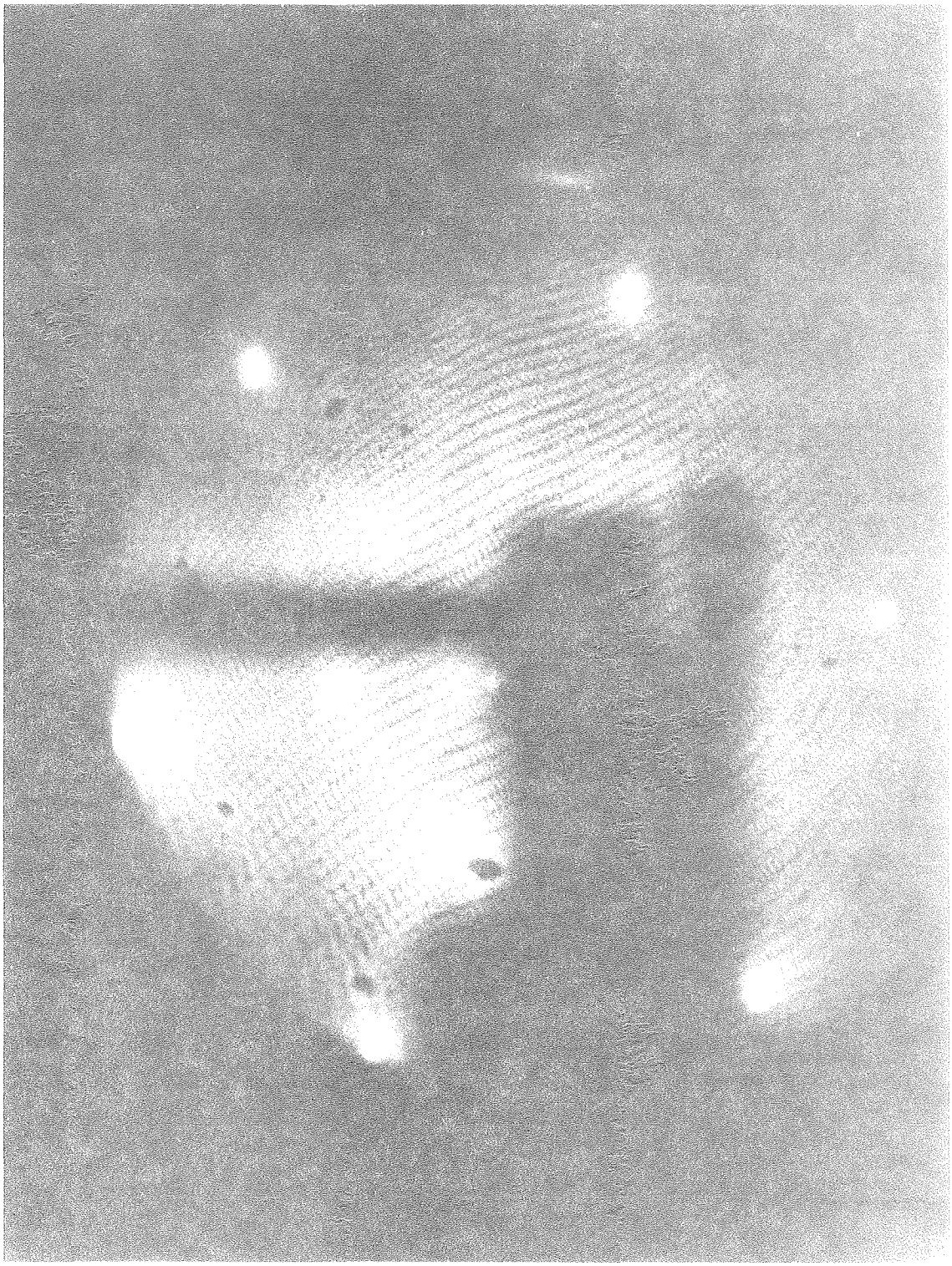

Figure 5a

XBB811-802

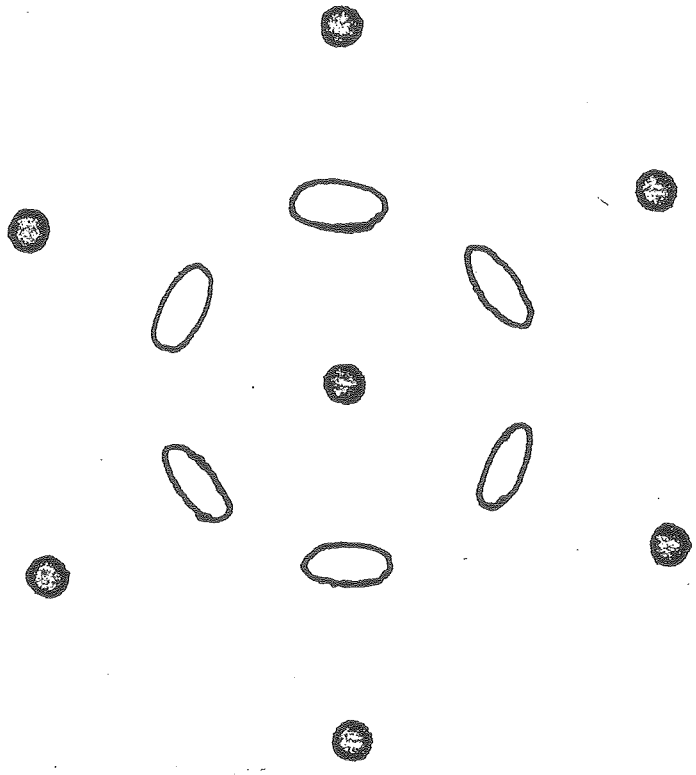

XBL 811-7806

Figure 5b

Figure 6a

XBB811-803

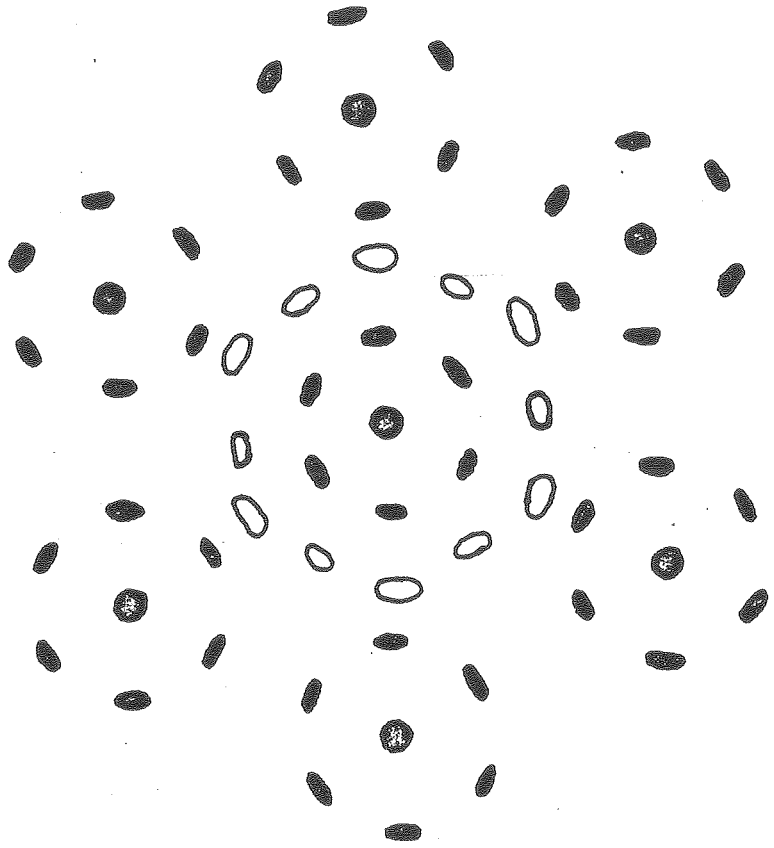

XBL 811-7805

Figure 6b

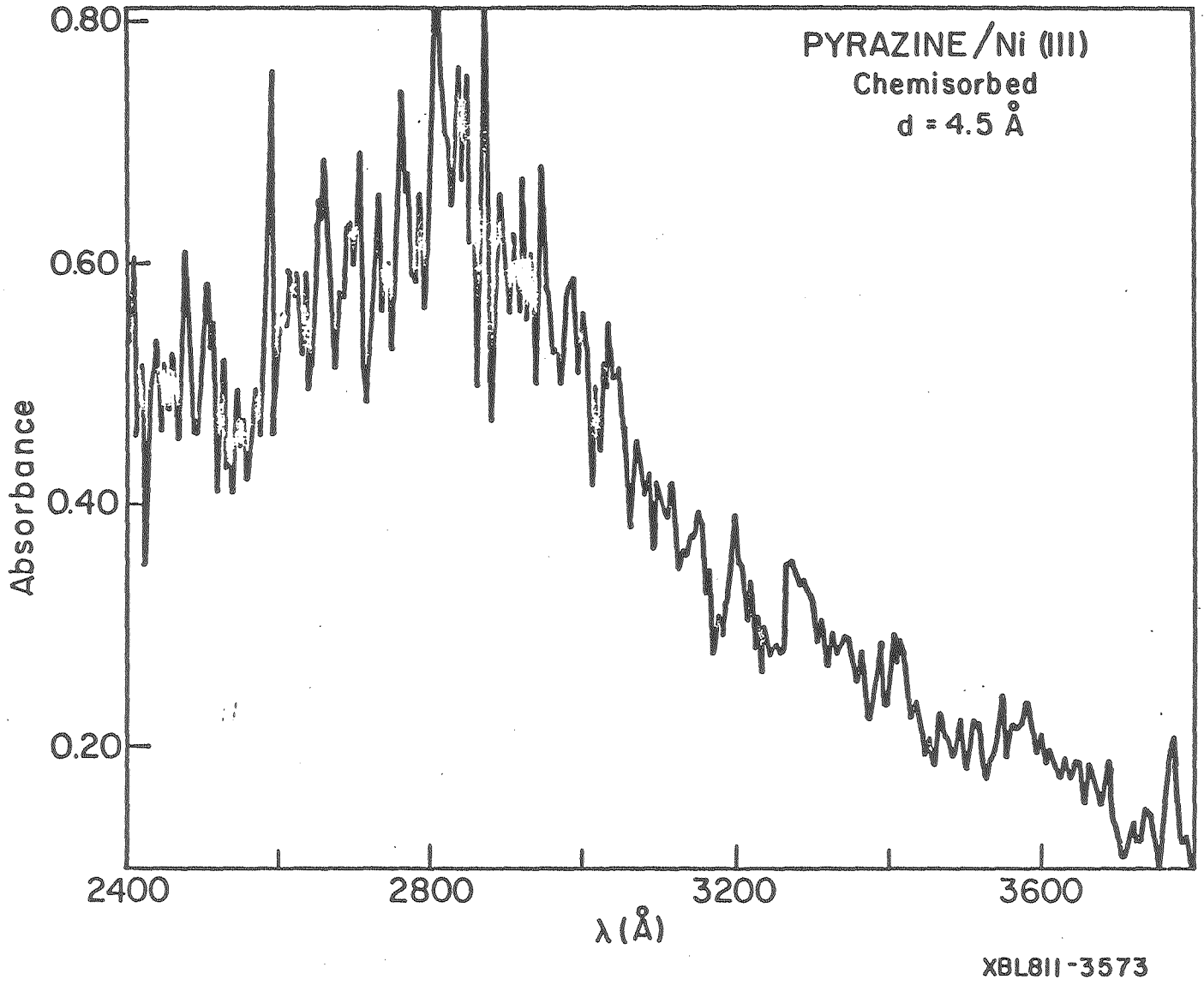
PYRAZINE/Ni (III)
Chemisorbed
d = 4.5 Å
0.80
0.60
0.40
0.20
Absorbance
2400
2800
3200
3600
λ(Å)
XBL811-3573

Figure 7

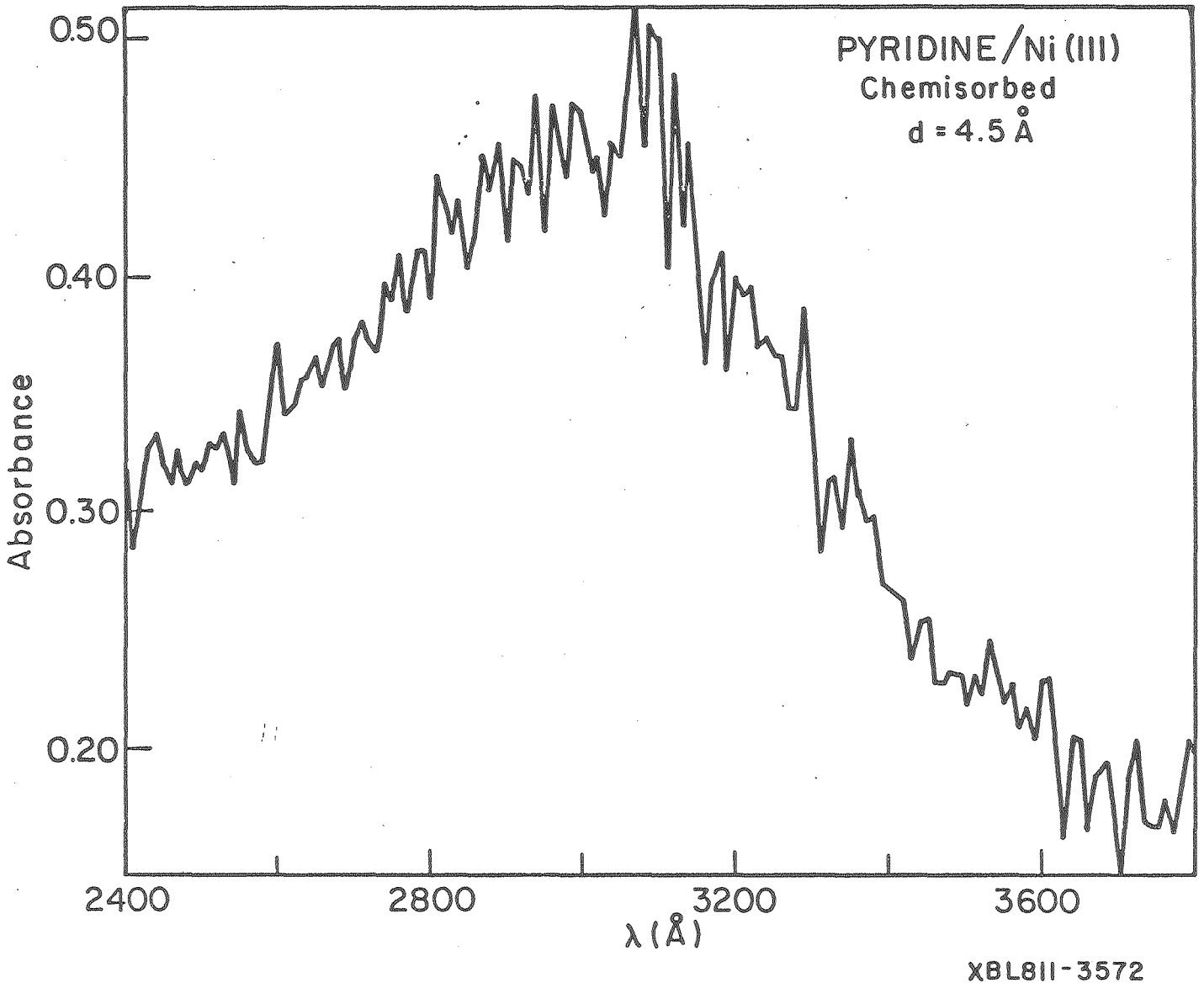
PYRIDINE/Ni (111)
Chemisorbed
d = 4.5 Å
0.50
0.40
0.30
0.20
Absorbance
2400
2800
3200
3600
λ (Å)
XBL811-3572

Figure 8

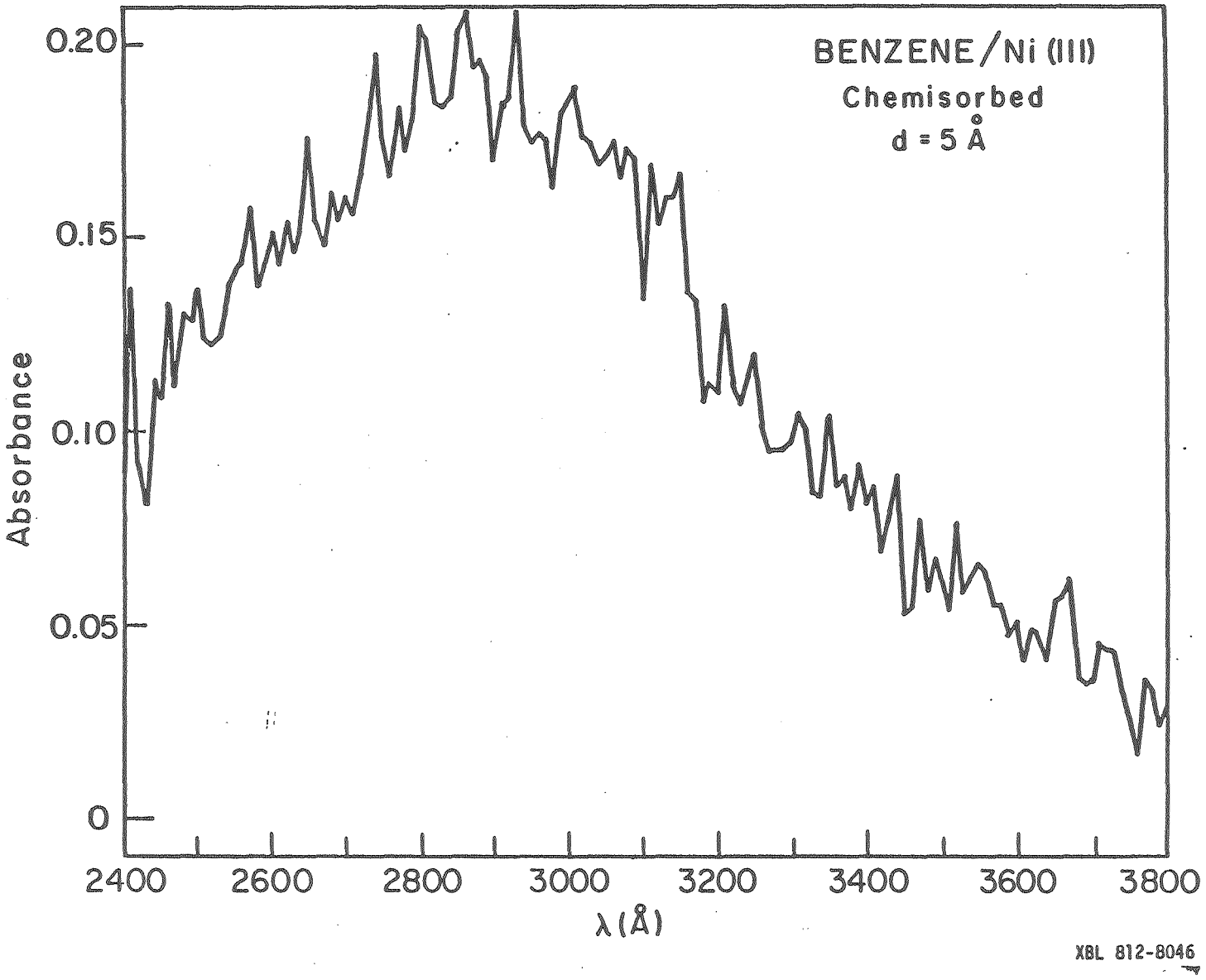
BENZENE/Ni (111)
Chemisorbed
d = 5 Å
Absorbance
0.20
0.15
0.10
0.05
0
2400
2600
2800
3000
3200
3400
3600
3800
λ(Å)
XBL 812-8046

Figure 9

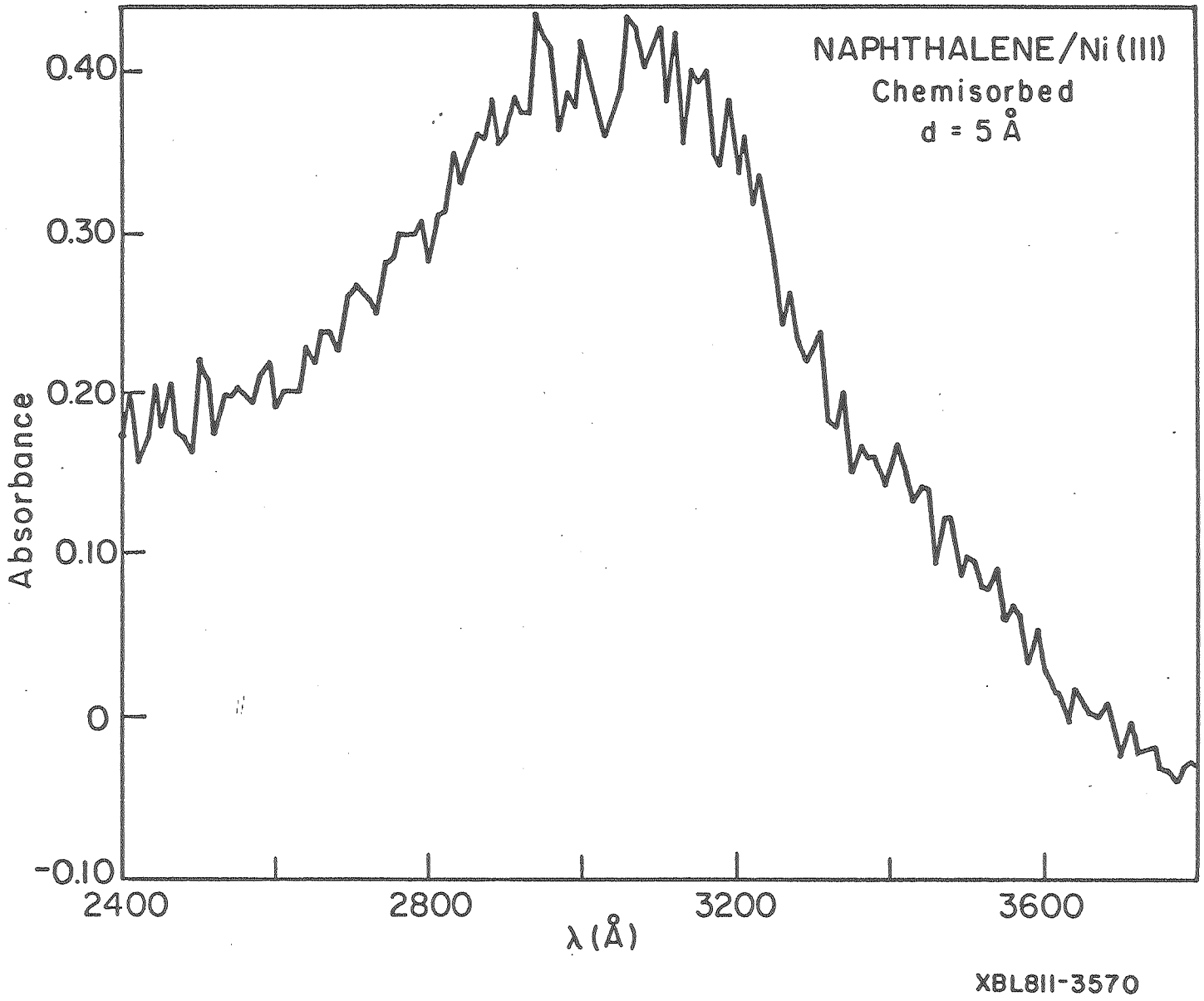
NAPHTHALENE/Ni(111)
Chemisorbed
d = 5 Å
0.40
0.30
0.20
0.10
0
-0.10
Absorbance
2400
2800
3200
3600
λ(Å)
XBL811-3570

Figure 10

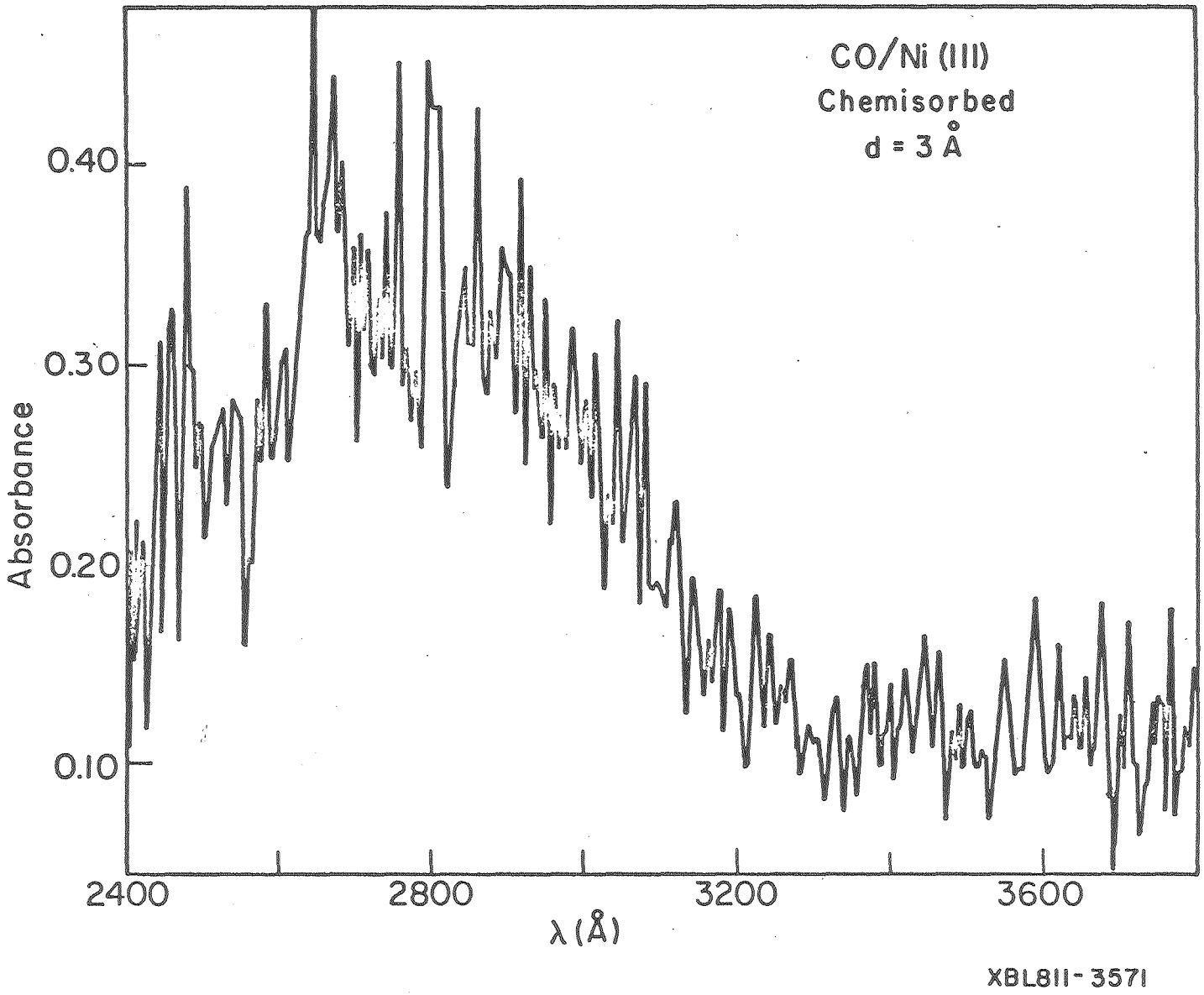
CO/Ni (111)
Chemisorbed
d = 3 Å
0.40
0.30
0.20
0.10
Absorbance
2400
2800
3200
3600
λ (Å)
XBL811-3571

Figure 11

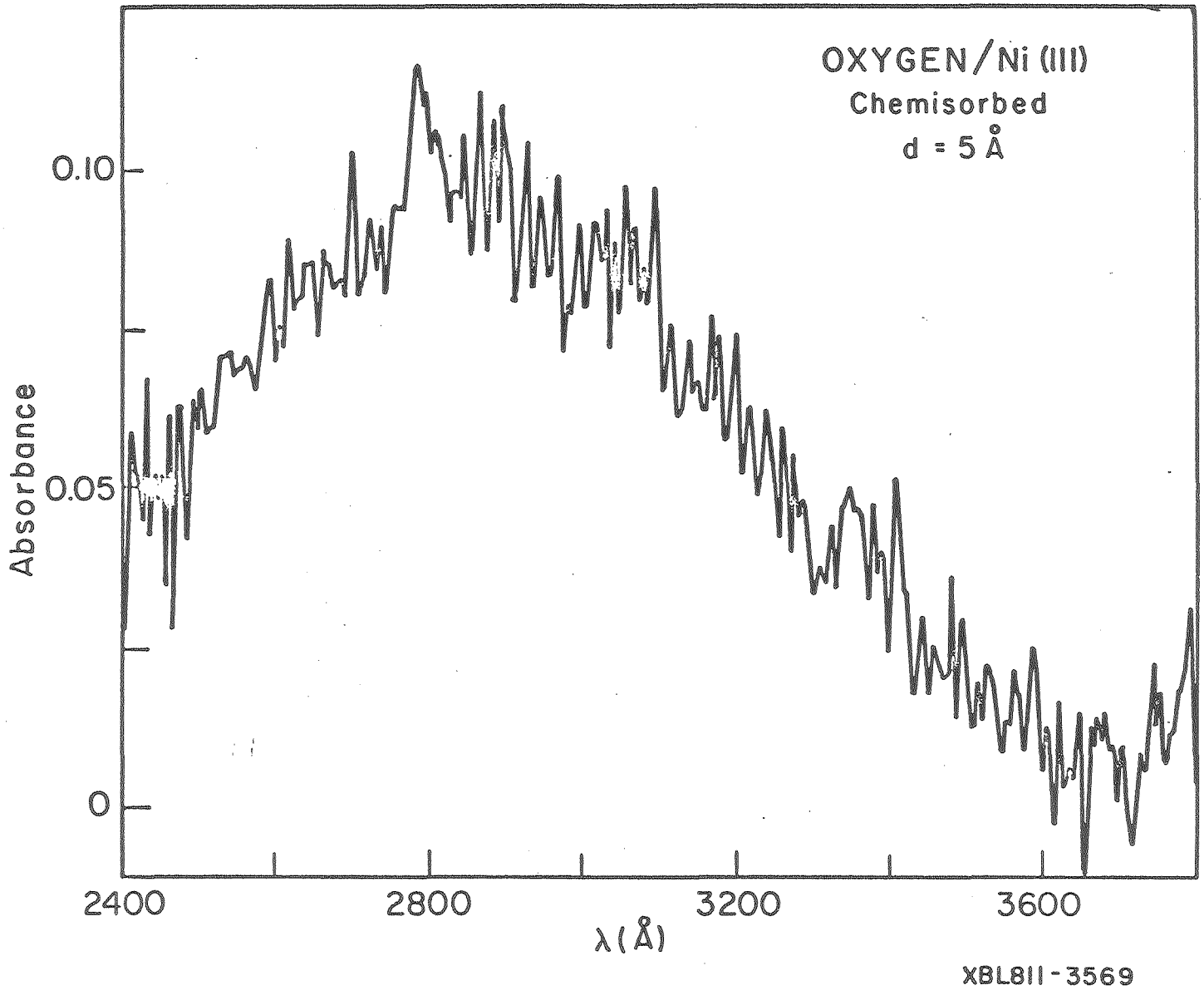
OXYGEN/Ni (111)
Chemisorbed
d = 5 Å
0.10
0.05
0
Absorbance
2400
2800
3200
3600
λ(Å)
XBL811-3569

Figure 12

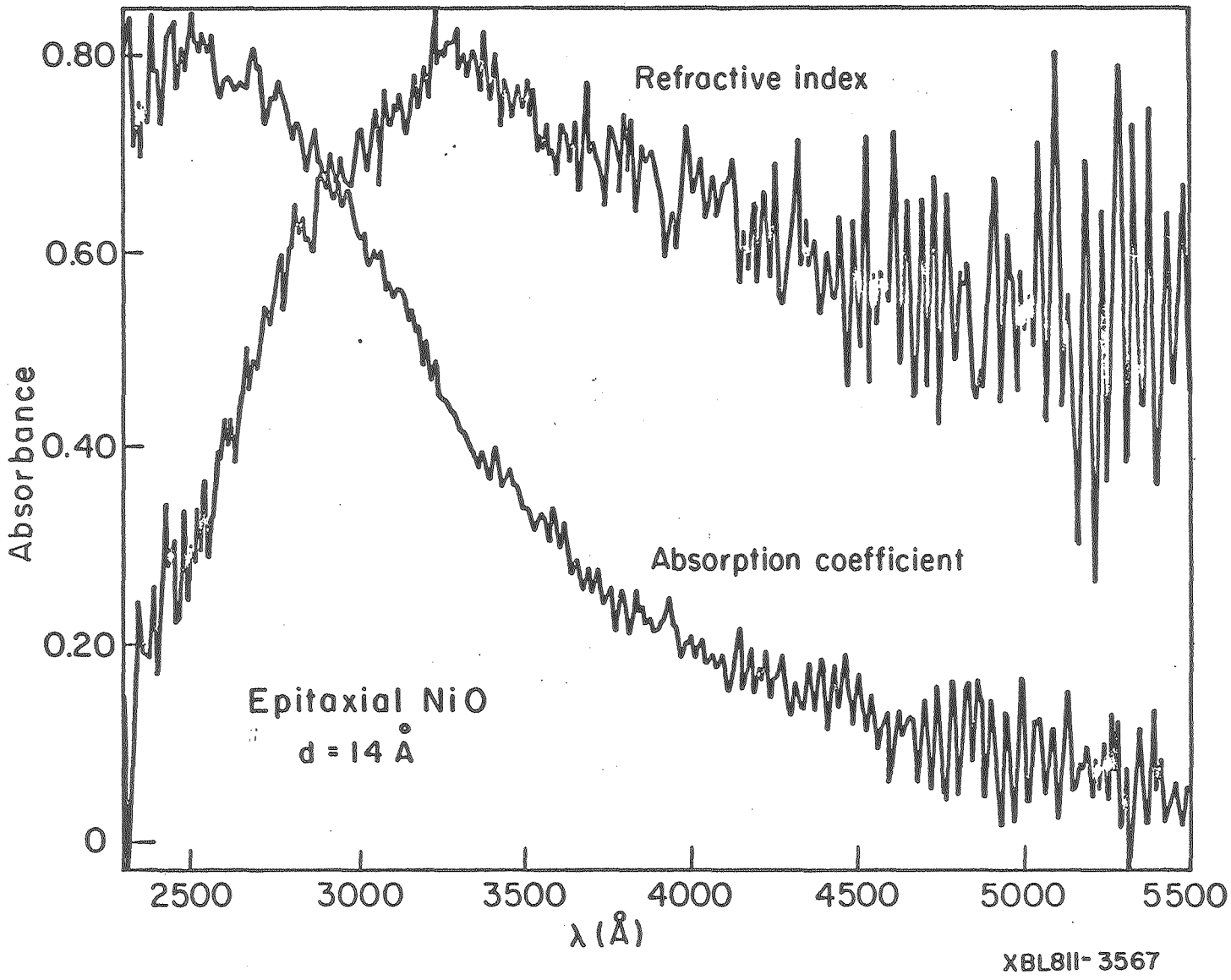
0.80
0.60
0.40
0.20
0
Absorbance
Refractive index
Absorption coefficient
Epitaxial NiO
d = 14 Å
2500
3000
3500
4000
4500
5000
5500
λ (Å)
XBL811-3567

Figure 13

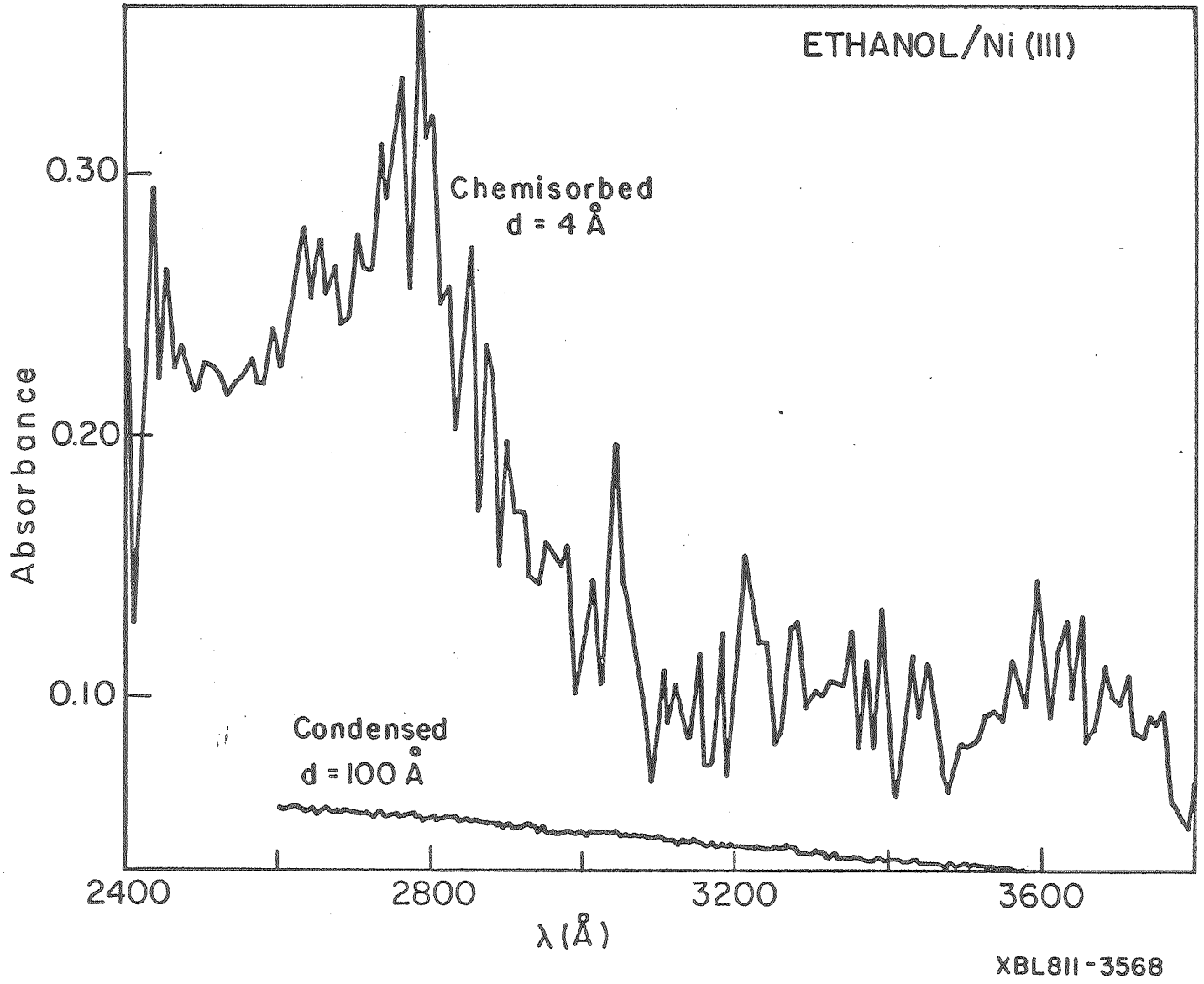
ETHANOL/Ni (111)
Chemisorbed
d = 4 Å
Condensed
d = 100 Å
Absorbance
0.30
0.20
0.10
2400
2800
3200
3600
λ (Å)
XBL811-3568

Figure 14

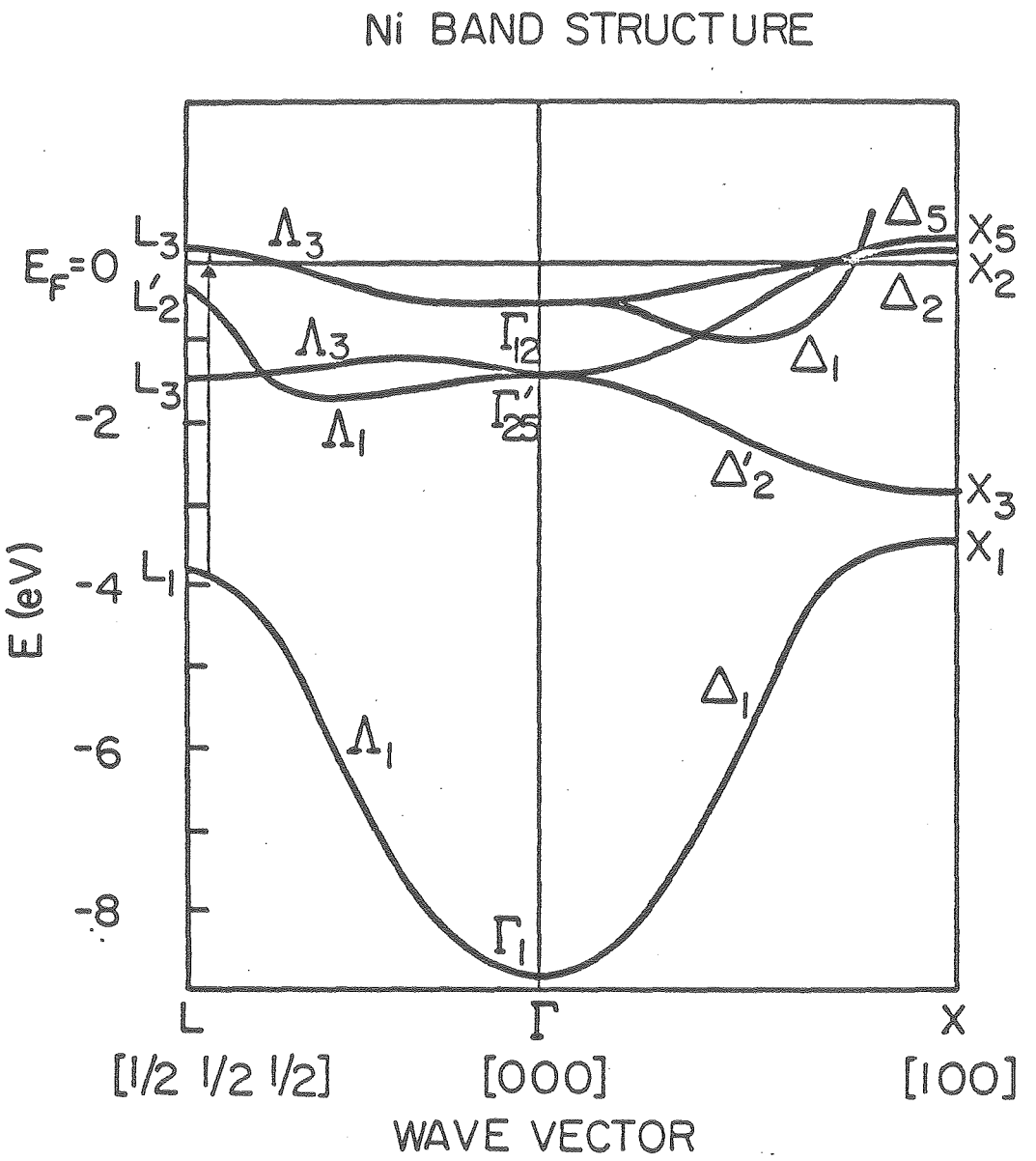
Ni BAND STRUCTURE
E_F=0
-2
-4
-6
-8
E (eV)
L_3
L'_2
L_3
L_1
Λ_3
Λ_3
Λ_1
Λ_1
Γ_{12}
Γ'_{25}
Γ_1
Δ_5
Δ_2
Δ_1
Δ'_2
Δ_1
X_5
X_2
X_3
X_1
L
Γ
X
[1/2 1/2 1/2]
[000]
[100]
WAVE VECTOR
XBL 818-6205

Figure 15